Biophysical Journal Volume 97 October 2009 1853–1863

Actin-Myosin Viscoelastic Flow in the Keratocyte Lamellipod

Boris Rubinstein,[†] Maxime F. Fournier,[‡] Ken Jacobson,[§] Alexander B. Verkhovsky,[‡] and Alex Mogilner[¶*]
[†]Stowers Institute for Medical Research, Kansas City, Missouri; [‡]Ecole Polytechnique Federale de Lausanne, Laboratory of Cell Biophysics, Lausanne, Switzerland; [§]Department of Cell and Developmental Biology, University of North Carolina School of Medicine, Chapel Hill, North Carolina; and [¶]Department of Neurobiology and Department of Mathematics, University of California, Davis, California

ABSTRACT The lamellipod, the locomotory region of migratory cells, is shaped by the balance of protrusion and contraction. The latter is the result of myosin-generated centripetal flow of the viscoelastic actin network. Recently, quantitative flow data was obtained, yet there is no detailed theory explaining the flow in a realistic geometry. We introduce models of viscoelastic actin mechanics and myosin transport and solve the model equations numerically for the flat, fan-shaped lamellipodial domain of keratocytes. The solutions demonstrate that in the rapidly crawling cell, myosin concentrates at the rear boundary and pulls the actin network inward, so the centripetal actin flow is very slow at the front, and faster at the rear and at the sides. The computed flow and respective traction forces compare well with the experimental data. We also calculate the graded protrusion at the cell boundary necessary to maintain the cell shape and make a number of other testable predictions. We discuss model implications for the cell shape, speed, and bi-stability.

INTRODUCTION

Many cells move on surfaces using flat motile appendages called lamellipodia (1). These appendages are made of a network of actin filaments (F-actin) enveloped by the cell membrane. The growth of filaments by polymerization at the lamellipodial periphery causes protrusion. Graded adhesion (firm at the front and weak at the rear) and contraction of the actin network lead to the forward translocation of the cell (Fig. 1). The cell body at the rear of the motile cell is often a passive cargo (2); indeed, lamellipodial fragments without a nucleus are able to crawl with shapes and speeds similar to intact cells (3,4). Thus, it is justified to focus on the lamellipod without the cell body. Lamellipodial contraction is mainly caused by myosin II motors (1,5) (later called simply ''myosin''), and it is the self-organization of the actin-myosin lamellipodial network that is responsible for the movements and forces of the motile cell that we aim to understand here in numerical detail.

Usually, the lamellipodial movements are complex, but fish and amphibian keratocytes, when present as single cells, are able to crawl on surfaces with remarkable speed (up to 1 μm per second) and persistence, while almost perfectly maintaining their shape (6,7). The keratocyte is canoe-shaped or fanlike, with a smooth-edged, flat lamellipodium at the anterior side of the cell body (Fig. 1) (6,7). Thus, the keratocyte lamellipodial shape is likely to represent the basic shape of the crawling cell in its pure form, determined solely by the actin network dynamics. The lamellipod is only a few tenths of a micron thick but is tens of microns long and wide, and contains a dense branched actin network (1,8).

A combination of the dendritic nucleation (1) and myosin-powered network contraction (5) models has been advanced to explain lamellipodial motility in broad strokes (reviewed extensively in the literature (1,6,7,9–11)): In the keratocyte, the steps of protrusion, graded adhesion, and retraction are continuous and simultaneous. At the center and sides of the leading edge, nascent actin filaments branch from the existing filaments and grow, thus pushing the lamellipodial boundary outward until these new filaments are capped. Since a new generation of growing filaments replaces the capped ones, the process is continuous. The filaments are distributed along the leading edge unevenly, with higher density at the center and lower at the sides (12–14). This leads to a graded rate of protrusion that is faster at the center, where the membrane resistance in terms of force per filament is lower, and slower at the sides, where the resistance per filament is higher. According to the geometric graded radial extension model (15), the lamellipodial boundary extends in a locally normal direction (Fig. 1 *B*), and thus the graded rate of actin growth, decreasing from the center to the sides, translates into the characteristic fanlike shape of the lamellipod.

Thousands of myosin molecules, each developing a pN-range force, are distributed throughout the cell (5). These forces do not perturb drastically the relatively stiff actin network in the front half of the lamellipod. However, the actin network disassembles throughout the lamellipod (16) and likely weakens mechanically toward the rear. At the same time, in the coordinate system of the moving cell, myosin molecules attached to the F-actin network are effectively swept to the rear, where they generate contractile stresses and collapse the isotropic actin network into a bipolar actin-myosin bundle at the very rear of the lamellipod (5,17) (Fig. 1 *A*). Subsequent musclelike sliding contraction of this bundle advances the rear boundary of the lamellipod and restrains the lamellipodial sides (Fig. 1 *B*). The actin filaments adhere to the surface on which the cell crawls through dynamic molecular complexes involving transmembrane

Submitted April 7, 2009, and accepted for publication July 13, 2009.

*Correspondence: mogilner@math.ucdavis.edu

Editor: Denis Wirtz.

0006-3495/09/10/1853/11 $2.00

doi: 10.1016/j.bpj.2009.07.020

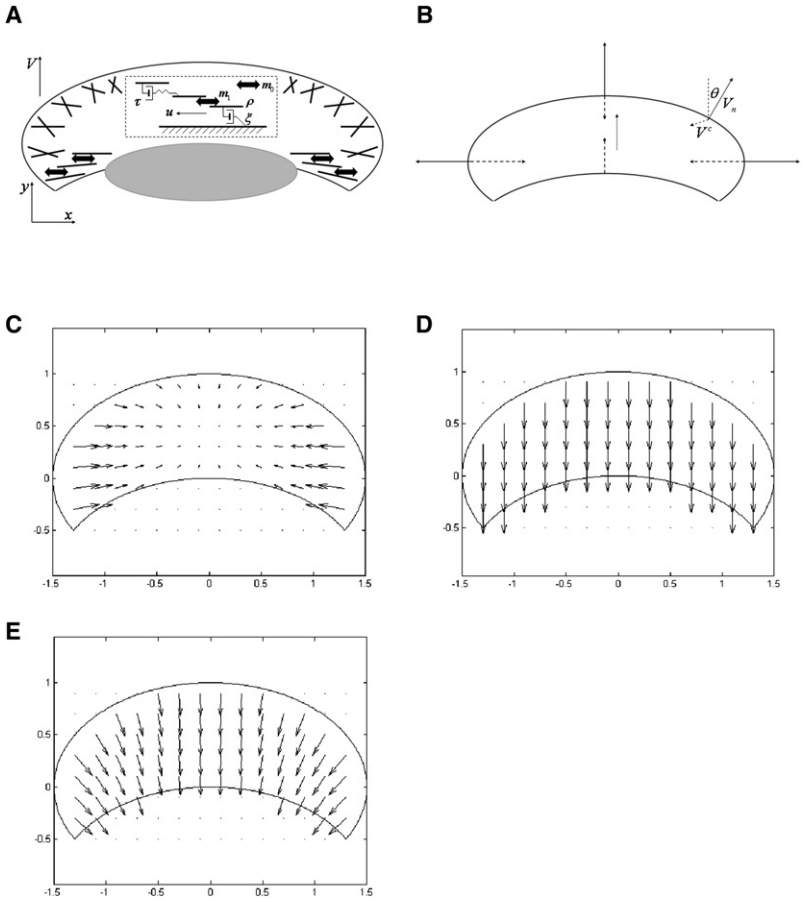

FIGURE 1 Two-dimensional model of the actin network flow. (*A*) Motile keratocyte cell, view from above. The cargo of the cell body is depicted by the gray ellipse at the rear. The lamellipod glides with the steady shape and velocity V, while the branched actin network (*crisscross segments*) grows at the leading edge and retracts at the rear due to the contractile action of myosin (*thick double-arrows*). (*Inset*) Mechanical model of the actin-myosin lamellipodial network. Actin filaments (segments, density ρ) glide with velocity u, undergo relative viscoelastic sliding (*spring* and *dashpot* in series, viscoelastic stress τ), and are contracted by working myosins (density m_1). Adhesion results in effective viscous drag (*dashpot*, density ξ). Myosin molecules cycle between the working and free (density m_0) states. (*B*) Hypothesized maintenance of the lamellipodial shape: The actin network grows at the front and sides (*solid arrows*), while the centripetal actin flow is fast at the rear and sides and slow at the front (*dashed arrows*). At the sides, the outward growth and inward flow cancel each other. At the rear, there is no actin growth, and the centripetal actin flow is equal to the cell speed (*dotted arrow*). The front advances with the cell speed equal to the difference between the local rates of actin growth and centripetal flow. To maintain the steady shape, the net local normal extension rate at the lamellipodial boundary has to obey the equation $(V_n - V^c \cdot \mathbf{n}) = V \times cos\theta$, where V_n is the local actin growth rate, V^c is the local actin centripetal flow velocity, n is the local normal unit vector, and θ is the angle between n and the direction of movement. (*C*) Characteristic map of the actin centripetal flow, $u(r)$, in the lab coordinate system. (*D*) In the framework of the steadily moving cell, there is the kinematic flow of F-actin to the rear with constant rate V equal to the cell speed. (*E*) In the framework of the cell, the actin-myosin network drift is the geometric sum, $(u(r) - V)$, of the flows shown in panels *C* and *D*. If $V > |u(r)|$, then the resulting drift sweeps the myosin to the rear.

adhesion receptors (9). These adhesion complexes are dense along a narrow rim at the leading edge (18), and in addition, there are two large adhesive regions at the rear corners of the lamellipod.

Recently, microscopy revealed how the lamellipodial actin network flows relative to the surface (19,17): the characteristic flow is centripetal, directed inward from the edges to the center of the cell (Fig. 1 *C*). The flow is fast, ~0.1 μm/s, at the sides and rear and slow, ~0.01 μm/s, at the front. This flow map suggests the following attractive hypothesis: the centripetal flow complements the graded protrusion in determining the shape and speed of the lamellipod by balancing the actin growth at the sides and pulling the actin network forward at the rear (Fig. 1 *B*). As a part of testing this hypothesis, mathematical modeling has to confirm that the qualitative ideas about the mechanisms of the myosin distribution and actin flow maintenance conforms with basic physics of actin-myosin transport and polymer gel mechanics. Thus, we set out to numerically reproduce the observed actin flow map, as well as the measured distribution of tractions that the moving cell exerts on the surface (2).

To do that, one has to choose appropriate mechanical properties of the malleable actin network that can have a wide range of rheologies depending on biological conditions. Generally, the actin network of the cell is viscoelastic, with very complex mechanical properties that can be approximated by a combination of Maxwell and Kelvin-Voight models (20–24). The viscoelastic rheology of actin gels, modeled in the literature (25–27), is nonlinear and sensitive to many parameters. Both purely elastic (28) and Kelvin (elastic with viscous transients) (29,30) models of the lamellipodial network were derived and simulated, but here we will use the Maxwell model such that if a constant force is applied to the actin network, then there is a short-term elastic response followed by a long-term viscous, flowlike behavior. This choice is justified by the observations of the stationary disklike keratocytes (31) and lamellipodial fragments (4), in which the actin network flows steadily and centripetally for many minutes under the action of constant contractile stress.

The myosin-powered movements of the cellular actin network were modeled before, starting from pioneering theory of reactive interpenetrating viscous flow that treated the cytoplasm as a two-phase fluid (32,33). Among several later efforts (29,34–37), one is especially relevant for our study: in Kruse et al. (35), the viscoelastic behavior in the ventral-dorsal cross-section of the lamellipod was modeled.

In a sense, Kruse et al. (35) addressed the dynamics of the lamellipod as seen from the side. Here, we model the viscoelastic actin-myosin dynamics in the keratocyte lamellipod as seen from above (Fig. 1 *A*), in a realistic two-dimensional geometry. Using the Maxwell model, we compute the actin flow, myosin distribution, and traction forces and compare the results with the experimental observations. Then, we discuss implications of the model predictions for the lamellipodial shape maintenance, which was earlier examined quantitatively with help of various models in the literature (13,28,38–41).

EXPERIMENTAL MEASUREMENTS OF THE FLOW AND ADHESION STRENGTH

Only F-actin flow was measured in the literature (17,19). To compare the measured flow rates with the theory and to estimates the adhesion strength distribution, we measured the actin network velocity in the migrating cell as described in Schaub et al. (17) and simultaneously measured the stress exerted on the elastic substrate (details will be reported elsewhere). Then, assuming that the adhesion has a viscous character, the adhesion strength distribution was computed at every spatial point as a ratio of the local traction force per unit area to the local actin network speed. The results are shown in Fig. 2 and discussed below.

Mathematical model of the myosin-powered flow of viscoelastic actin network

Mechanics of the actin-myosin network

Several studies have proposed a hyperbolic model describing the properties of polymeric viscolelastic fluids (42,43). We use a modification of this model containing diffusionlike (44,45) terms. The model variables and parameters are gathered in the Supporting Material. The equation of motion in such a model has the form

$$\rho\left[\frac{\partial \mathbf{u}}{\partial t} + (\mathbf{u}\cdot\boldsymbol{\nabla})\mathbf{u}\right] = -\boldsymbol{\nabla}p + \boldsymbol{\nabla}\cdot[2(1-\alpha)\eta\mathbf{D}(\mathbf{u}) + \boldsymbol{\tau}] + \mathbf{F}.$$

Here ρ is the F-actin density, η denotes the effective viscosity of the F-actin network, and $\mathbf{u}$ is the local velocity of the actin

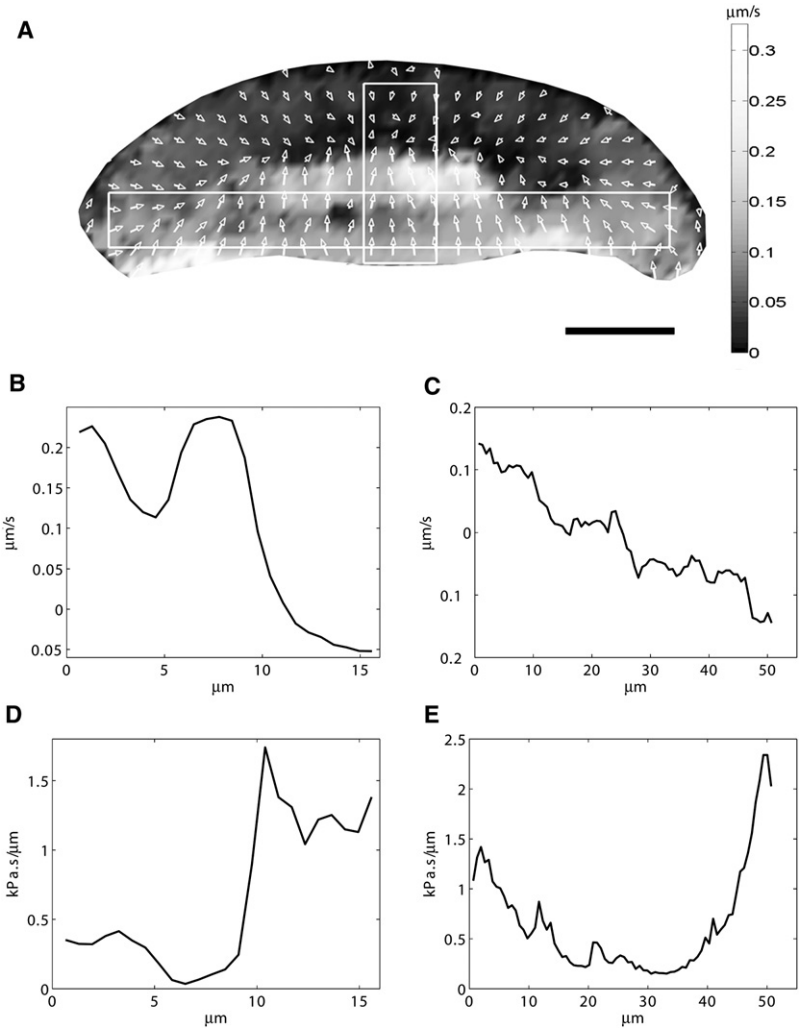

FIGURE 2 Experimentally measured distribution of actin network velocity and adhesion strength in migrating keratocyte. (*A*) Two-dimensional actin velocity map obtained as described in Schaub et al. (17). Bar, 10 μm. (*B*) Distribution profile of posterior-anterior component of actin velocity along posterior-anterior direction. Zero position corresponds to the back of the cell; velocity values for each distance from the back of the cell were averaged within the vertical rectangular region indicated on velocity map in panel *A*. (*C*) Distribution profile of lateral component of actin velocity along lateral direction. Zero position corresponds to the left side of the cell; velocity values for each distance from the left side were averaged within the horizontal rectangular region indicated on velocity map in panel *A*. Posterior-anterior (*D*) and lateral (*E*) distributions of adhesion strength parameter in, respectively, vertical and horizontal rectangular regions shown in panel *A*. Experimental determination of adhesion parameter will be described elsewhere. Briefly, actin network velocity and stress exerted on the substrate were measured simultaneously, and adhesion parameter was computed at every position of the cell as a ratio of the substrate stress to the actin network speed.

network in the lab coordinate system. The right-hand side describes the local forces: p is pressure; the second term is the sum of the divergence of viscous and viscoelastic stresses explained below; and the last term is responsible for the external body force,

$$\mathbf{F} = \boldsymbol{\nabla} \cdot \boldsymbol{\tau}^{\mathrm{myo}} + \mathbf{F}_{\mathrm{adh}}.$$

The latter in our model is generated by

1. The divergence of the myosin contractile stress, $\boldsymbol{\tau}^{\mathrm{myo}}$, and
2. The effective viscous drag, $\mathbf{F}_{\mathrm{adh}}$, between the actin network, adhesive complexes and surface to which the lamellipod adheres and is described below.

Note that the mechanics equations in our model are written in the lab coordinate system, not in the framework of the steadily moving cell.

We restrict ourselves to the case of very low Reynolds numbers, which is usual for cell biology, so we drop the nonlinear term $(\mathbf{u} \cdot \nabla)\mathbf{u}$ in the equation of motion. Furthermore, we drop the pressure term based on the following considerations. In the two-phase interpenetrative flow model (32), the pressure originates from the incompressibility of the combined polymer/fluid system. Separately, however, the polymer mesh is compressible, and when the local polymer density changes, the fluid fraction of the cytoplasm flows in or out of the polymer mesh. There is a limiting case, in which the polymer dynamics can be effectively uncoupled from the fluid dynamics (33), namely, when Darcy friction forces between the porous polymer mesh and fluid squeezing through it can be neglected. These forces can be estimated as the characteristic F-actin movement rate, ~0.1 μm/s, divided by the hydraulic permeability of the cytoskeleton, ~0.01 $\mu\mathrm{m}^3/(\mathrm{pN} \times \mathrm{s})$ (46), so the order of magnitude of respective stress is ~10 $\mathrm{pN}/\mu\mathrm{m}^2$. Myosin contractile stress in keratocyte (and viscoelastic polymer stresses balancing it) is ~100 $\mathrm{pN}/\mu\mathrm{m}^2$ (2,47). In this limit, the Darcy forces and fluid hydrostatic pressure can be neglected if the polymer movements are considered. (These forces are not negligible if one models fluid movements (48), but here we are not addressing them.) In addition, it is feasible that the lamellipodial actin mesh consists of a denser ventral layer of polymers and a less dense dorsal layer (49). Then, fluid would be largely squeezed out of the ventral layer and move almost freely near the dorsal surface. This would diminish gradients of the fluid hydrostatic pressure and make the dense F-actin network effectively compressible.

Thus, we use the equation of motion in the form

$$\rho \frac{\partial \mathbf{u}}{\partial t} = \boldsymbol{\nabla} \cdot [2(1-\alpha)\eta \mathbf{D}(\mathbf{u}) + \boldsymbol{\tau}] + \boldsymbol{\nabla} \cdot \boldsymbol{\tau}^{\mathrm{myo}} + \mathbf{F}_{\mathrm{adh}}. \tag{1}$$

In the expression for the internal stress in the polymer network, $(2(1–\alpha)\eta\mathbf{D}(\mathbf{u}) + \tau)$, the first term describes the viscous part of the stress tensor proportional to the rate-of-deformation tensor, $\mathbf{D}$,

$$(\boldsymbol{\nabla}\mathbf{u})_{\mathrm{ij}} = \frac{\partial u_{\mathrm{j}}}{\partial x_{\mathrm{i}}}, \quad D_{\mathrm{ij}} = \frac{1}{2}\left(\frac{\partial u_{\mathrm{i}}}{\partial x_{\mathrm{j}}} + \frac{\partial u_{\mathrm{j}}}{\partial x_{\mathrm{i}}}\right) = \frac{1}{2}(\boldsymbol{\nabla}\mathbf{u} + (\boldsymbol{\nabla}\mathbf{u}))^{\mathrm{T}}. \tag{2}$$

Parameter α determining a non-Newtonian fraction of viscosity can be defined by the ratio of two timescales characteristic for the polymer mesh—the retardation time λ_{r} (relaxation time for strain) to the relaxation time λ (relaxation time for stress): $\alpha = 1 - (\lambda_{\mathrm{r}}/\lambda)$ (44).

The equation describing the viscoelastic part of the stress tensor, $\boldsymbol{\tau}$, has the form

$$\boldsymbol{\tau} + \lambda\left[\frac{\partial \boldsymbol{\tau}}{\partial t} + \mathbf{u} \cdot \boldsymbol{\nabla}\boldsymbol{\tau} - \boldsymbol{\tau} \cdot \boldsymbol{\nabla}\mathbf{u} - (\boldsymbol{\nabla}\mathbf{u})^{\mathrm{T}} \cdot \boldsymbol{\tau}\right] = 2\alpha\eta\mathbf{D}. \tag{3}$$

The dynamics described by this equation corresponds to the Upper Convected Maxwell model of a viscoelastic fluid (44), which in the limiting case $\lambda = 0$ reduces to the standard linear relation between the stress tensor and the deformation rate tensor for Newtonian fluids obeying the Navier-Stokes equation. Equation 3 is the simplest variant out of a dozen or so model equations used for the description of the non-Newtonian fluids (44). In the extreme case of a purely non-Newtonian fluid ($\alpha = 1$), this equation becomes hyperbolic. The boundary condition to Eqs. 1–3 is a zero normal component of stress tensor at the lamellipodial boundary,

$$[2(1-\alpha)\eta\mathbf{D} + \boldsymbol{\tau} + \boldsymbol{\tau}^{\mathrm{myo}}] \cdot \mathbf{n} = \mathbf{0}, \tag{4}$$

where $\mathbf{n}$ is the locally normal unit vector at the boundary.

Characteristic parameters and scales

We choose the characteristic lamellipodial size, L ~10 μm, as the scale of distance and cell speed, and V ~0.2 μm/s as the scale of the velocity, so L/V ~50 s is the scale of time. Maximum F-actin density at the leading edge, ρ_0, is the scale of density (measured in units of $\mathrm{g}/\mu\mathrm{m}^3$; its actual value does not appear to be important since the Reynolds number is low). Finally, we choose $\eta_0 V$, where η_0 is the characteristic viscosity of the F-actin network at the leading edge (its value in units of pN × s/μm is estimated below), as the scale of force.

Using these scales, we introduce the nondimensional quantities, for which we keep the same notations, as

$$\mathbf{u} \Rightarrow \frac{\mathbf{u}}{V}, \ \mathbf{r} \Rightarrow \frac{\mathbf{r}}{L}, \ t \Rightarrow \frac{tV}{L}, \ \rho \Rightarrow \frac{\rho}{\rho_0}, \ \eta \Rightarrow \frac{\eta}{\eta_0}, \ \boldsymbol{\tau} \Rightarrow \frac{\boldsymbol{\tau}L}{\eta_0 V}, \ \mathbf{F} \Rightarrow \frac{\mathbf{F}L^2}{\eta_0 V}.$$

Note that we consider the two-dimensional problem appropriate for the flat lamellipodial geometry, so the dimensions of the body force and stress are $\mathrm{pN}/\mu\mathrm{m}^2$ and $\mathrm{pN}/\mu\mathrm{m}$, respectively. In the nondimensional form, the mechanics model equations read

$$Re\,\rho\,\frac{\partial \mathbf{u}}{\partial t} = \boldsymbol{\nabla}\cdot\left[(1-\alpha)\eta\left(\boldsymbol{\nabla}\mathbf{u} + (\boldsymbol{\nabla}\mathbf{u})^{\mathrm{T}}\right) + \boldsymbol{\tau}\right] + \boldsymbol{\nabla}\cdot\boldsymbol{\tau}^{\mathrm{myo}} + \mathbf{F}_{\mathrm{adh}}, \tag{5}$$

$$\boldsymbol{\tau} + De\left[\frac{\partial \boldsymbol{\tau}}{\partial t} + \mathbf{u}\cdot\boldsymbol{\nabla}\boldsymbol{\tau} - \boldsymbol{\tau}\cdot\boldsymbol{\nabla}\mathbf{u} - (\boldsymbol{\nabla}\mathbf{u})^{\mathrm{T}}\cdot\boldsymbol{\tau}\right] = \alpha\eta\left(\boldsymbol{\nabla}\mathbf{u} + (\boldsymbol{\nabla}\mathbf{u})^{\mathrm{T}}\right), \tag{6}$$

$$\left[(1-\alpha)\eta\left(\boldsymbol{\nabla}\mathbf{u} + (\boldsymbol{\nabla}\mathbf{u})^{\mathrm{T}}\right) + \boldsymbol{\tau} + \boldsymbol{\tau}^{\mathrm{myo}}\right]\cdot\mathbf{n} = \mathbf{0} \text{ at the boundary.} \tag{7}$$

Here $Re = \rho_0 VL/\eta_0$ is the Reynolds number, and $De = \lambda V/L$ is the Deborah number. The Reynolds number in cell biology is very small compared to 1 (27,32,48); in the simulations we use $Re = 0.1$. Note that we keep and use the inertial term proportional to the Reynolds number just as an artificial time-stepping to relax the system of equations to their steady-state values. The presence of this term does not affect the model: we checked that decreasing the Reynolds number by an order of magnitude does not alter the results.

The viscoelastic relaxation time was measured to be approximately a few seconds (22–24) (or even ~0.1 s (20)), much smaller than the characteristic timescale L/V ~50 s, so the Deborah number De ~0.02–0.2 is small; in simulations we used $De = 0.2$. This means that the elastic memory in the lamellipod fades rapidly, and the system is effectively viscous. To the best of our knowledge, there are no direct reports of numerical values for parameter α for the actin gels. In the Supporting Material, we estimate this parameter α ~0.9–0.99 based on data in the literature (23,24).

Finally, let us note that there are no rapid (second scale) transient flows or large spatial gradients in flows or stresses in the cell movements. We checked that retaining the viscoelastic terms in the model equations introduce only ~10% corrections to the purely viscous solutions. Qualitatively, these corrections are equivalent to slightly damping the myosin-generated stress and resulting decrease in the magnitude and gradients of the flow. Thus, our model suggests that treating actin network as a complex fluid versus a viscous, Newtonian fluid would give comparable results.

We specify the terms $\mathbf{F}_{\mathrm{adh}}$, $\boldsymbol{\tau}^{\mathrm{myo}}$, and the spatial variations of the F-actin density and viscosity below. We use the value of the actin network viscosity ~2×10^3 Pa × s (20) to estimate the characteristic viscosity in the two-dimensional model by multiplying this value by the characteristic thickness of the lamellipod, 0.2 μm (8), so $\eta_0 = 400$ pN × s/μm. Considering that the maximum observed gradients of the flow rate in the lamellipod are ~0.1 (μm/s)/μm, the characteristic scale of stress in our model (product of the viscosity and flow rate gradient) is tens of pN per micron. This stress is of the same order of magnitude as the observed myosin-generated contractile stress (2,47).

Myosin transport and stress generation

We consider the steady movement of the lamellipod with the constant velocity $\mathbf{V}$ (Fig. 1) and assume that the myosin motors are either associated with or dissociated from the F-actin network. We denote the density of these subpopulations of the motors as $m_1(\mathbf{r}, t)$ and $m_0(\mathbf{r}, t)$, respectively. The actin-associated working motors are assembled into clusters, with multiple motor heads producing power-strokes and generating the contractile stress. These motors drift, together with the F-actin network, with the rate $(-\mathbf{V} + \mathbf{u}(\mathbf{r}, t))$. Note that here we consider myosin dynamics in the framework of the cell moving forward with constant speed. Therefore, in the cell framework, in addition to drifting with F-actin with the rate $\mathbf{u}$ (in the lab coordinate system), myosin is also swept to the rear with the constant rate $(-\mathbf{V})$ (Fig. 1 *D*). We assume that the free motors (dissociated from the actin network) diffuse in the cytoplasm with diffusion coefficient D, that the working motors detach with the constant rate k_0, and that the free motors attach with the constant rate k_1. We neglect the possibility that there is a small convective flow of the fluid fraction of the cytoplasm due to the cell motion. The equations of motion for the myosin densities are

$$\frac{\partial m_1}{\partial t} = -k_1 m_1 + k_0 m_0 - \boldsymbol{\nabla}\cdot((\mathbf{u}-\mathbf{V})m_1), \tag{8}$$

$$\frac{\partial m_0}{\partial t} = k_1 m_1 - k_0 m_0 + D\nabla^2 m_0. \tag{9}$$

The free myosin density has to obey the no-flux boundary conditions at the entire lamellipodial boundary. The natural boundary condition for the hyperbolic equation for the working myosin is zero density at the part of the boundary where the effective drift $(-\mathbf{V} + \mathbf{u})$ moves myosin inward. Mathematically, this part of the boundary can be identified by the sign of the dot product of the effective drift with the outward unit normal vector: $(-\mathbf{V} + \mathbf{u}(\mathbf{r}, t)) \cdot \mathbf{n}(\mathbf{r}, t) < 0$.

The term $\boldsymbol{\tau}^{\mathrm{myo}}$ in Eq. 1 describes actin-myosin contractile stress (32,50,51). Following Herant et al. (32) and interpreting data reported in Janson et al. (52), we assume that this macroscopic stress is isotropic, like a negative hydrostatic pressure in the cytoskeleton, so only the diagonal components of the stress tensor, equal to each other, are nonzero. We assume that the magnitude of stress is proportional to the working myosin density $\boldsymbol{\tau}^{\mathrm{myo}} = \kappa m_1(\mathbf{r}, t)$. The proportionality coefficient κ is chosen so that at the characteristic total average myosin density, the contractile stress is 100 pN/μm^2 (2,47). In the two-dimensional model, we have to multiply this stress by the lamellipodial thickness, ~0.2 μm, to get $\boldsymbol{\tau}^{\mathrm{myo}}$ ~ 20 pN/μm.

F-actin turnover and viscosity

We assume that the F-actin is polymerized at the leading edge and depolymerized with a constant rate elsewhere

across the lamellipod (16), so the F-actin density is governed by the reaction-drift equation:

$$\frac{\partial \rho}{\partial t} = -\nabla \cdot ((\mathbf{u} - \mathbf{V})\rho) - \gamma\rho. \quad (10)$$

Note that, same as the myosin dynamics, the actin kinetics are considered in the framework of the cell moving forward with constant speed. Here γ is the disassembly rate, the order of magnitude of which can be surmised from the observation that the actin filaments' half-life in the keratocyte lamellipodium is tens of seconds (16). In the simulations, we use $\gamma = 0.03$/s. The boundary condition for Eq. 10 is the constant F-actin density $\rho = \rho_0$ at the part of the boundary where the effective drift is inward (same as that for the working myosin equation). We scale the actin equation using the scales of density, time, and distance introduced above. In the simulations, we assume that the viscosity is linearly proportional to the actin density (so that $\eta = \eta_0$ at $\rho = \rho_0$). Finally, note that recent data (17) suggests that the disassembly rate is not constant, but rather increasing toward the rear, perhaps accelerated there by the myosin action. There is no difficulty in using such spatially nonuniform rate in the computations; however, trial simulations showed that this does not change results qualitatively, so for simplicity, we kept the disassembly uniform.

Adhesion distribution

The exact mechanics of adhesion between the cell and substrate is unknown, so we choose the simplest description of the interaction between the actin network and the surface through a viscous drag force on the cell that is proportional to the actin flow velocity:

$$\mathbf{F}_{\text{adh}} = -\xi(\mathbf{r}) \times \mathbf{u}(\mathbf{r}).$$

This choice for the drag force has been used in a number of other models for cell motility (36,37,53).

The line plots of the adhesion strength (Fig. 2, *D* and *E*) suggest that the effective adhesion drag coefficient, $\xi(\mathbf{r})$, correlates with the observed higher density of the adhesions at the narrow rim along the leading edge and strong adhesion regions at the rear corners of the lamellipodia, in addition to weak evenly distributed adhesions throughout the lamellipod (18,54). Mathematically, we modeled this distribution with the linear superposition of the Gaussian bell-shaped functions centered along the leading edge with additional functions of similar shapes at the rear side corners of the lamellipod (Fig. 3 *A*). The range of the spatial spread of the strong adhesion near the leading edge and rear sides was equal to 1 μm. The characteristic magnitude of the adhesion viscous drag can be estimated by dividing the characteristic traction force density, ~100 pN/μm^2 (2), by the characteristic flow rate, ~0.1 μm/s, so $\xi_0 \sim 1000$ pN $\times$ s/μm^3. This estimate is in agreement with our measurement (Fig. 2, *D* and *E*).

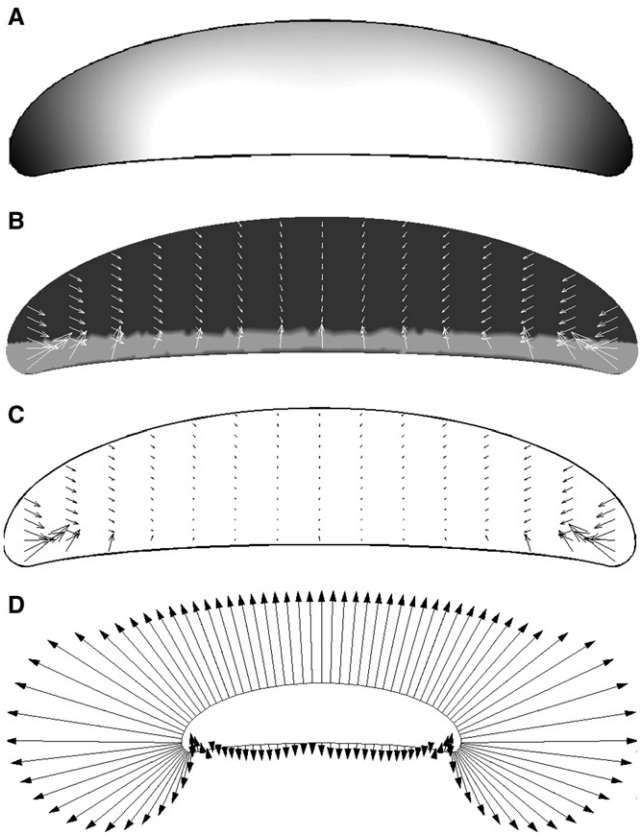

FIGURE 3 Actin flow and traction forces. (*A*) Spatial distribution of the adhesion strength used in the calculations (*dark shading* corresponds to stronger adhesion). (*B*) Open arrows show the computed actin flow map. Shading shows the myosin density (*light* corresponds to high density). (*C*) Computed distribution of the traction forces. (*D*) Actin growth rate distribution at the lamellipodial boundary required to maintain the steady shape.

ANALYSIS OF THE MODEL

Myosin distribution

The myosin distribution in the lamellipod can be understood from first analyzing the one-dimensional example, in which the equations for the myosin densities are solved on the anterior-posterior segment of length L: $y < 0 < L$, where 0 and L are the coordinates of the rear and front, respectively. In this case, the equations of motion for the myosin densities read

$$\frac{\partial m_1}{\partial t} = -k_1 m_1 + k_0 m_0 - \frac{\partial}{\partial y}((u(y) - V)m_1), \quad (11)$$

$$\frac{\partial m_0}{\partial t} = k_1 m_1 - k_0 m_0 + D\frac{\partial^2 m_0}{\partial y^2}. \quad (12)$$

Choosing the lamellipodial size L as the length scale, $1/k_1$ as the timescale, and $k_0 M/(k_0 + k_1)$ and $k_1 M/(k_0 + k_1)$ as the scales of the densities of working and free myosin, respectively, we can rewrite the myosin equations in the nondimensional form,

$$\frac{\partial \tilde{m}_1}{\partial \tilde{t}} = -\tilde{m}_1 + \tilde{m}_0 - \left(\frac{V}{k_1 L}\right)\frac{\partial}{\partial \tilde{y}}\left(\left(\frac{u}{V} - 1\right)\tilde{m}_1\right), \quad (13)$$

$$\frac{\partial \tilde{m}_0}{\partial \tilde{t}} = \left(\frac{k_0}{k_1}\right)\left[\tilde{m}_1 - \tilde{m}_0 + \left(\frac{D}{k_0 L^2}\right)\frac{\partial^2 \tilde{m}_0}{\partial \tilde{y}^2}\right], \quad (14)$$

where $\tilde{t} = k_1 t$, $\tilde{y} = y/L$, $\tilde{m}_1 = (k_0 + k_1)m_1/(k_0 M)$, $\tilde{m}_0 = (k_0 + k_1)/(k_1 M)$, and M is the total average myosin density. The boundary conditions in one dimension are no flux at both front and rear for the free myosin and zero working myosin density at the front ($y = L$), providing the cell speed is greater than the magnitude of the F-actin flow: $V > u(y)$.

Only two nondimensional parameters, $(V/k_1 L)$ and $(D/k_2 L^2)$, determine the steady spatial distribution of the myosin (only timescales, not spatial effects, depend on the ratio k_0/k_1). The first of these parameters, $(V/k_1 L)$, defines how far a working myosin molecule drifts before it dissociates from the F-actin, and the second one, $(D/k_2 L^2)$, quantifies how far a free myosin molecule diffuses before it associates with the F-actin. In the Supporting Material, we demonstrate that if $(V/k_1 L) >> 1$, then most of the stress-generating myosin is at the rear in the steadily motile cell. As $V \sim 0.2$ μm/s, and $L \sim 10$ μm, the dissociation rate has to be $k_1 < 0.01$/s for this regime to be valid. Furthermore, in the Supporting Material we show that in two dimensions most of myosin is also at the rear, and model its distribution with constant density along the narrow zone near the rear boundary (Fig. 3 *B*).

RESULTS

One-dimensional F-actin flow

To build intuition about the actin network behavior predicted by the model, it is useful to neglect the two-dimensional effects and consider one-dimensional caricature model of the rectangular lamellipodial domain with uniform adhesion and myosin density decreasing linearly from its maximum value at the rear to zero at the front (Fig. 4 *A*). In this case, the anterior-posterior and lateral distributions of the flow velocities can be found analytically. We will use the subscripts x (y) to denote the spatial derivative $\partial/\partial x$ ($\partial/\partial y$). The anterior-posterior F-actin density can be found by solving the steady state equation $[(V - u)\rho]_x - \gamma\rho = 0$. Assuming that we can neglect the flow rate u compared to the cell speed V, other than very close to the rear, we have $V\rho_x - \gamma\rho \approx 0$. The respective solution predicts the density $\rho \approx \rho_0 \exp[(\gamma/V)(x - L)]$ exponentially decreasing away from the front over the characteristic distance $V/\gamma \sim 10$ μm, in qualitative agreement with the observations in the front half of the lamellipod (4,5).

Neglecting the small terms proportional to Deborah number, the viscoelastic stress along the lateral cross-section can be found easily: $\tau \approx 2\alpha\eta u_x$. Neglecting the small terms proportional to Reynolds number, we can rewrite the equation of actin flow in the lateral direction in the form

$$[2(1 - \alpha)\eta u_x + \tau + m]_x = \xi u,$$

with the boundary conditions given by $2(1 - \alpha)\eta u_x + \tau + m = 0$. Here m denotes the contractile stress scalar proportional to the working myosin density. Finally, substituting the equation for stress into the equation of motion and boundary condition, we derive the simple one-dimensional lateral flow equation $[2\eta u_x + m]_x = \xi u$ with the boundary conditions given by $2\eta u_x + m = 0$.

This equation can be easily solved analytically along the lateral cross-section (*AB* in Fig. 4 *A*) from $x = -L$ to $x = L$ for constant viscosity η, adhesion ξ, and myosin stress m. Because the myosin stress along the lateral cross-section is

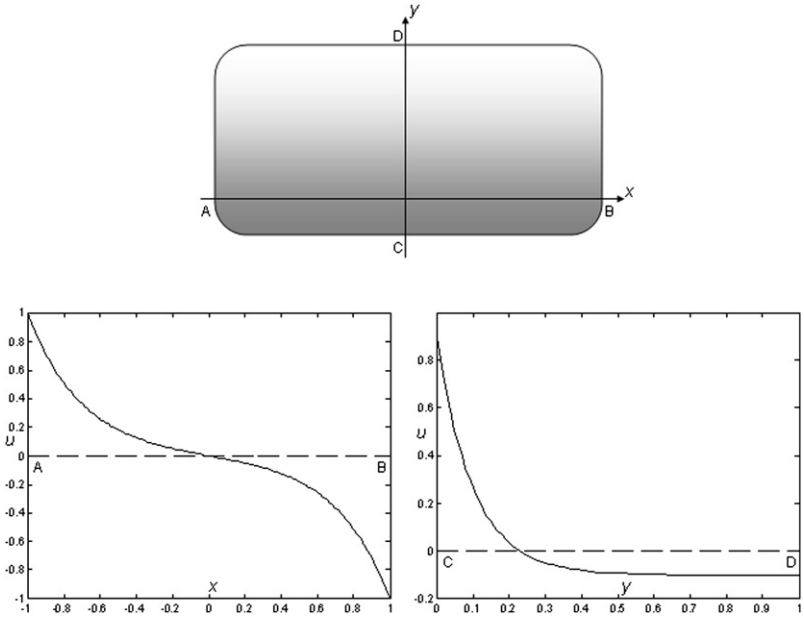

FIGURE 4 Simplified one-dimensional model of the actin-myosin flow. If the two-dimensional effects are neglected in the rectangular domain with uniform adhesion and myosin linearly biased to the rear (*darker shading* corresponds to higher myosin), then the anterior-posterior and lateral distributions of the flow velocities can be found analytically. (*Left/right bottom line plots*) Flow rates from the left to the right side and from the rear to the front, respectively. The flow rate is in units of the maximum rate at the side; the unit of distance is the half-width of the lamellipodial domain.

constant, the flow equation simplifies to $2\eta u_{xx} = \xi u$. Introducing the characteristic length scale on which the flow is fast near the cell sides, $l = \sqrt{2\eta/\xi}$, the solution has the form

$$u \approx \frac{-m}{\sqrt{\eta\xi/2}} \left(\exp[(x-L)/l] - \exp[(-x-L)/l]\right).$$

The predicted actin flow rate shown in Fig. 4 *A* is directed inward and antisymmetric relative to the center (positive at the left and negative at the right). It stays very low near the center and increases rapidly at the sides. The maximum flow rate at the sides is proportional to the myosin contractile stress and inversely proportional to the square roots of the actin viscosity and adhesion strength.

Similarly, the flow can be calculated along the posterior-anterior cross-section (*CD* in Fig. 4, with the rear at $y = 0$ and front at $y = L$) with constant viscosity η, adhesion ξ, and myosin stress distributed as $m = \overline{m}(1 - y/L)$. In this case, the flow equation has the form

$$2\eta u_{yy} - (\overline{m}/L) = \xi u,$$

with the boundary condition at the front $u_y = 0$ and that at the rear $2\eta u_y + \overline{m} = 0$. The approximate analytical solution to this equation has the form

$$u \approx \frac{\overline{m}}{\sqrt{\eta\xi/2}} [\exp(-y/l) - (l/L)].$$

The predicted actin flow shown in Fig. 4 *A* is retrograde, constant and small throughout most of the central part of the lamellipod. The magnitude of this retrograde flow, $\sim (\overline{m}/(\xi L))$, is proportional to the myosin contractile stress, inversely proportional to the adhesion strength and is viscosity-independent. This flow also has to decrease with increasing cell size. Near the rear, the flow becomes anterograde and increases exponentially to significant magnitude $\sim \overline{m}/\sqrt{\xi\eta}$, which is similar to the inward flow at the sides and has similar functional dependencies on myosin, adhesion and viscosity.

These predicted flow distributions are in qualitative agreements with the experimental line plots (Fig. 2, *B* and *C*). The measured inward flow at the sides decreases slower, more linearly, toward the center, than predicted. Furthermore, the anterograde flow at the rear is more irregular and extends farther to the front than predicted. However, these discrepancies are likely due to the unknown, more complex and dynamic than assumed, distribution of the myosin, contractile stresses and, most importantly, effective actin viscosity at the rear. In addition, note that the rear peak of the flow corresponds to the fast flow under the cell body; then, there is a slowing down at the boundary between the cell body and the lamellipod, and again a fast flow at the rear of the lamellipod. The model, strictly speaking, is applicable to the lamellipod only.

Maps of the centripetal flow and traction forces

We scaled and nondimensionalized the model equations as described above and solved them numerically (using Femlab software—from The MathWorks, Natick, MA—and various initial conditions on a desktop PC computer) on the lamellipod-shaped domains. The numerical solutions converged asymptotically to the stable steady density and velocity distributions shown in Fig. 3 *B*.

The F-actin density is predicted by the solutions to decrease in a near-exponential fashion from the front to the rear of the lamellipod (not shown), in agreement with the observations (4). At the very rear, this decrease is stopped by the myosin-powered contraction. We obtained the characteristic graded centripetal actin flow distribution similar to that measured (Fig. 2 and Fig. 3 *B*): the flow is directed roughly to the center, slow at the center front, and faster at the sides and rear. The flow decreases from the periphery toward the center of the lamellipod.

While the viscous adhesive forces are applied to the sliding actin network of the motile cell, opposite forces are applied to the surface on which the cell crawls. In the framework of the model, these tractions forces can be computed by multiplying the local assumed adhesion strength by the local computed F-actin velocity. The result is shown in Fig. 3 *C*. Numerical integration confirmed that the geometric sum of the traction forces is equal to zero: total force from the substrate on the cell is balanced just by drag on the cell from the aqueous environment. The map of the traction forces has roughly the same pattern as that of the F-actin flow. However, the traction forces are disproportionately great at the rear corners of the lamellipod because great inward flow speed there is multiplied by the high adhesion strength. These great rear corner forces are directed inward and slightly skewed forward and are balanced by widely distributed low density traction in the front half of the lamellipod. This predicted pattern is in qualitative agreement with the experimental measurements (2). In the Supporting Material, we describe how the flow changes when the model parameters are varied.

Lamellipodial shaping by the balance between the actin growth and centripetal flow

The authors of the graded radial extension model (18) discovered a geometric relation between the steady shape of the lamellipodial boundary and the local rate of boundary extension. Generalized to the case when the actin network grows in a locally normal direction to the boundary with a rate $V_n(s)$, where s is the arc length coordinate along the boundary, and flows inward at the lamellipodial periphery with the rate $\mathbf{V}^c(s)$, this geometric relation has the form

$$(V_n(s) - \mathbf{V}^c(s)\mathbf{n}(s)) = V \times \cos\theta\,(s),$$

where $\mathbf{n}(s)$ is the local normal unit vector, and θ is the angle between $\mathbf{n}$ and the direction of movement (Fig. 1 *B*).

The focus of this study is on explaining the actin centripetal flow in the cells of given shapes, therefore the actin growth velocity along the boundary is not a part of the model. However, one important question is what the actin growth velocity along the boundary has to be to maintain the given steady shape in the presence of the centripetal actin flow computed for this shape. We used the geometric relation of the graded radial extension model, as well as the lamellipodial shape, computed values of the centripetal actin flow $\mathbf{V}^{\mathbf{c}}(s)$, and cell speed employed in the calculations depicted in Fig. 3 to calculate the spatial distribution of the actin growth rates required to maintain this shape. The result is shown in Fig. 3 *D*. Almost constant actin growth is needed at the front, and almost zero growth at the rear. This roughly corresponds to the simplest cell motility scenario illustrated in Fig. 1 *B*; however, the actin growth at the sides has to be very rapid in this case to cancel the fast inward flow at the sides. In addition, at the rear sides, the actin growth has to be distributed with some rapid spatial fluctuations (Fig. 3 *D*). In the future, simulations of the free boundary lamellipodial domain will be needed to estimate whether the shape remains stable without these fluctuations.

DISCUSSION

We formulated and solved numerically the equations describing coupled myosin transport and myosin-powered viscoelastic flow of the F-actin network in a realistic two-dimensional lamellipodial geometry. The model is based on the assumptions of isotropic myosin contraction and viscous adhesion behavior. The model suggests that treating the lamellipodial network as a complex fluid versus a viscous, Newtonian fluid gives comparable results, which is due to the relatively slow cell movements compared to the actin mesh relaxation time. The computational results compare qualitatively very well with experimental measurements (2,17,19) and our data. Indeed, the model predicts the centripetal direction of the F-actin flow. In the anterior-posterior direction the flow in the front of the cell is slow and retrograde, while at the rear the flow is fast and anterograde (17,19). The lateral flow at the sides is directed inward—rapid at the lateral edges of the cell and slow in the central part of the cell. The predicted map of the traction forces also agrees with the measurements qualitatively (2).

In agreement with the model prediction, the centripetal actin flow in cells treated with blebbistatin, which reduces myosin-based contractility, is reduced (13,17), whereas in cells treated with calyculin, which increases the action of myosin, the inward flow accelerates (13). In addition, experimental studies reported positive correlation between the adhesive close contacts at the leading edge of the cell and the cell speed (55). This agrees with the theoretical prediction that if adhesion at the front is stronger, then the retrograde flow at the front is slower. Effectively, this produces a more rapid rate of protrusion; at the same time, the anterograde flow at the rear is increased to maintain pace with the more rapid protrusion at the front.

Our model suggests, following the qualitative scenario in Verkhovsky et al. (3) and refining simplified physical arguments given earlier (40), how the myosin helps the cell to maintain the polarized motile state. In the framework of the rapidly motile cell, myosin is swept to the rear, where it contracts the actin network weakened by the depolymerization generating rapid centripetal flow that pulls the rear forward and the sides inward. These actions help prevent the sides from spreading and allow the rear to maintain pace with the protruding front. On the other hand, when the cell slows down significantly, our model predicts that myosin will no longer be swept to the rear because the centripetal actin flow that myosin generates would now move the working myosin inward everywhere. In this case, the centripetal flow would be radially symmetric; thus, if the actin network now grows uniformly at the boundary, the steady shape of the cell or its lamellipodial fragment becomes disklike, and the cell or fragment become stationary in agreement with experimental observations (3,31). We will test the model on the free boundary domain to investigate local stability of these symmetric nonmotile and asymmetric motile states and how global perturbations switch the cell between them. Some additional mechanisms maintaining the cell shape and movement are discussed in the Supporting Material.

We modeled explicitly here and in the past (reviewed in (11)) two steps of the migration cycle—protrusion and contraction—but simply assumed that the distribution of the adhesion strengths was similar to the observed adhesion density pattern. One possible explanation for this observed adhesion pattern is that the adhesion complexes are targeted to the nascent growing actin filaments at the leading edge (56); in addition, strong inward pulling action at the lamellipodial sides can lead to growth and strengthening of the adhesions there (57). We did not include adhesion dynamics into the model because they are not understood well. Furthermore, some observations indicate nonlinearity in adhesion regulation by myosin contraction (58). In the future, realistic adhesion dynamics, provided by new measurements, should be coupled to the actin-myosin equations. Indeed, the greatest obstacle to improving the detailed quantitative predictable capabilities of the model is not, in fact, the theoretical issues discussed above, but the lack of quantitative biophysical data. Nevertheless, the ability of the model to reproduce qualitatively a few essential features of keratocyte actomyosin network dynamics and traction patterns is encouraging.

SUPPORTING MATERIAL

Supporting text and two tables are available at http://www.biophysj.org/biophysj/supplemental/S0006-3495(09)01241-7.

We are grateful to K. Keren for fruitful discussions.

This work was supported by National Institutes of Health GLUE grant ''Cell Migration Consortium'' (No. NIGMS U54 GM64346) to A.M. and K.J., and by National Science Foundation grant No. DMS-0315782 to A.M.; A.B.V. and M.F.F. were supported by Swiss National Science Foundation grant No. 3100A0-112413.

REFERENCES

1. Pollard, T. D., and G. G. Borisy. 2003. Cellular motility driven by assembly and disassembly of actin filaments. *Cell*. 112:453–465.
2. Oliver, T., M. Dembo, and K. Jacobson. 1999. Separation of propulsive and adhesive traction stresses in locomoting keratocytes. *J. Cell Biol.* 145:589–604.
3. Verkhovsky, A. B., T. M. Svitkina, and G. G. Borisy. 1999. Network contraction model for cell translocation and retrograde flow. *Biochem. Soc. Symp.* 65:207–222.
4. Verkhovsky, A. B., T. M. Svitkina, and G. G. Borisy. 1999. Self-polarization and directional motility of cytoplasm. *Curr. Biol.* 9:11–20.
5. Svitkina, T. M., A. B. Verkhovsky, K. M. McQuade, and G. G. Borisy. 1997. Analysis of the actin-myosin II system in fish epidermal keratocytes: mechanism of cell body translocation. *J. Cell Biol.* 139:397–415.
6. Rafelski, S. M., and J. A. Theriot. 2004. Crawling toward a unified model of cell mobility: spatial and temporal regulation of actin dynamics. *Annu. Rev. Biochem.* 73:209–239.
7. Keren, K., and J. Theriot. 2007. Biophysical aspects of actin-based motility in fish epithelial keratocytes. *In* Cell Motility. P. Lenz, editor. Springer, New York.
8. Abraham, V. C., V. Krishnamurthi, D. L. Taylor, and F. Lanni. 1999. The actin-based nanomachine at the leading edge of migrating cells. *Biophys. J.* 77:1721–1732.
9. Vicente-Manzanares, M., D. J. Webb, and A. R. Horwitz. 2005. Cell migration at a glance. *J. Cell Sci.* 118:4917–4919.
10. Carlsson, A. E., and D. Sept. 2008. Mathematical modeling of cell migration. *Methods Cell Biol.* 84:911–937.
11. Mogilner, A. 2009. Mathematics of cell motility: have we got its number? *J. Math. Biol.* 58:105–134.
12. Lacayo, C. I., Z. Pincus, M. M. VanDuijn, C. A. Wilson, D. A. Fletcher, et al. 2007. Emergence of large-scale cell morphology and movement from local actin filament growth dynamics. *PLoS Biol.* 5:e233.
13. Keren, K., Z. Pincus, G. M. Allen, E. L. Barnhart, G. Marriott, et al. 2008. Mechanism of shape determination in motile cells. *Nature.* 453:475–480.
14. Grimm, H. P., A. B. Verkhovsky, A. Mogilner, and J.-J. Meister. 2003. Analysis of actin dynamics at the leading edge of crawling cells: implications for the shape of keratocyte lamellipodia. *Eur. Biophys. J.* 32:563–577.
15. Lee, J., A. Ishihara, J. A. Theriot, and K. Jacobson. 1993. Principles of locomotion for simple-shaped cells. *Nature.* 362:167–171.
16. Theriot, J. A., and T. J. Mitchison. 1991. Actin microfilament dynamics in locomoting cells. *Nature.* 352:126–131.
17. Schaub, S., S. Bohnet, V. M. Laurent, J.-J. Meister, and A. B. Verkhovsky. 2007. Comparative maps of motion and assembly of filamentous actin and myosin II in migrating cells. *Mol. Biol. Cell.* 18:3723–3732.
18. Lee, J., and K. Jacobson. 1997. The composition and dynamics of cell-substratum adhesions in locomoting fish keratocytes. *J. Cell Sci.* 110:2833–2844.
19. Vallotton, P., G. Danuser, S. Bohnet, J.-J. Meister, and A. B. Verkhovsky. 2005. Tracking retrograde flow in keratocytes: news from the front. *Mol. Biol. Cell.* 16:1223–1231.
20. Bausch, A. R., F. Ziemann, A. A. Boulbitch, K. Jacobson, and E. Sackmann. 1998. Local measurements of viscoelastic parameters of adherent cell surfaces by magnetic bead microrheometry. *Biophys. J.* 75:2038–2049.
21. Keller, M., R. Tharmann, M. A. Dichtl, A. R. Bausch, and E. Sackmann. 2003. Slow filament dynamics and viscoelasticity in entangled and active actin networks. *Philos. Transact. A Math. Phys. Eng. Sci.* 361:699–711.
22. Kole, T. P., Y. Tseng, I. Jiang, J. L. Katz, and D. Wirtz. 2005. Intracellular mechanics of migrating fibroblasts. *Mol. Biol. Cell.* 16:328–338.
23. Wottawah, F., S. Schinkinger, B. Lincoln, R. Ananthakrishnan, M. Romeyke, et al. 2005. Optical rheology of biological cells. *Phys. Rev. Lett.* 94:098103.
24. Panorchan, P., J. S. Lee, T. P. Kole, Y. Tseng, and D. Wirtz. 2006. Microrheology and ROCK signaling of human endothelial cells embedded in a 3D matrix. *Biophys. J.* 91:3499–3507.
25. Liverpool, T. B., A. C. Maggs, and A. Ajdari. 2001. Viscoelasticity of solutions of motile polymers. *Phys. Rev. Lett.* 86:4171–4174.
26. Kruse, K., J. F. Joanny, F. Jülicher, J. Prost, and K. Sekimoto. 2004. Asters, vortices, and rotating spirals in active gels of polar filaments. *Phys. Rev. Lett.* 92:078101.
27. Bottino, D. C., and L. J. Fauci. 1998. A computational model of amoeboid deformation and locomotion. *Eur. Biophys. J.* 27:532–539.
28. Rubinstein, B., K. Jacobson, and A. Mogilner. 2005. Multiscale two-dimensional modeling of a motile simple-shaped cell. *SIAM J. MMS.* 3:413–439.
29. Gracheva, M. E., and H. G. Othmer. 2004. A continuum model of motility in amoeboid cells. *Bull. Math. Biol.* 66:167–193.
30. Kim, J. S., and S. X. Sun. 2009. Continuum modeling of forces in growing viscoelastic cytoskeletal networks. *J. Theor. Biol.* 256:596–606.
31. Yam, P. T., C. A. Wilson, L. Ji, B. Hebert, E. L. Barnhart, et al. 2007. Actin-myosin network reorganization breaks symmetry at the cell rear to spontaneously initiate polarized cell motility. *J. Cell Biol.* 178:1207–1221.
32. Herant, M., W. A. Marganski, and M. Dembo. 2003. The mechanics of neutrophils: synthetic modeling of three experiments. *Biophys. J.* 84:3389–3413.
33. Dembo, M., F. Harlow, and W. Alt. 1984. The biophysics of cell surface motility. *In* Cell Surface Dynamics: Concepts and Models. C. De Lisi, A. Perelson, and F. Wiegel, editors. Marcel Dekker, New York.
34. Yang, L., J. C. Effler, B. L. Kutscher, S. E. Sullivan, D. N. Robinson, et al. 2008. Modeling cellular deformations using the level set formalism. *BMC Syst. Biol.* 2:68.
35. Kruse, K., J. F. Joanny, F. Julicher, and J. Prost. 2006. Contractility and retrograde flow in lamellipodium motion. *Phys. Biol.* 3:130–137.
36. Larripa, K., and A. Mogilner. 2006. Transport of a 1D viscoelastic actin-myosin strip of gel as a model of a crawling cell. *Physica A.* 372:113–123.
37. Zajac, M., B. Dacanay, W. A. Mohler, and C. W. Wolgemuth. 2008. 2008 Depolymerization-driven flow in nematode spermatozoa relates crawling speed to size and shape. *Biophys. J.* 94:3810–3823.
38. Maree, A. F., A. Jilkine, A. Dawes, V. A. Grieneisen, and L. Edelstein-Keshet. 2006. Polarization and movement of keratocytes: a multiscale modeling approach. *Bull. Math. Biol.* 68:1169–1211.
39. Satyanarayana, S. V., and A. Baumgaertner. 2004. Shape and motility of a model cell: a computational study. *J. Chem. Phys.* 121:4255–4265.
40. Kozlov, M. M., and A. Mogilner. 2007. Model of polarization and bi-stability of cell fragments. *Biophys. J.* 93:3811–3819.
41. Satulovsky, J., R. Lui, and Y.-l. Wang. 2008. Exploring the control circuit of cell migration by mathematical modeling. *Biophys. J.* 94:3671–3683.
42. Phelan, F. R., M. F. Malone, and H. H. Winter. 1989. A purely hyperbolic model for unsteady viscoelastic flow. *J. Non-Newt. Fluid Mech.* 32:197–224.
43. Edwards, B. J., and A. N. Beris. 1990. Remarks concerning hyperbolic viscoelastic fluid models. *J. Non-Newt. Fluid Mech.* 36:411–417.

44. Bird, R. B., R. C. Armstrong, and O. Hassager. 1987. Dynamics of Polymeric Liquids. John Wiley and Sons.

45. Prilutski, G., R. K. Gupta, T. Sridhar, and M. E. Ryan. 1983. Model viscoelastic liquids. *J. Non-Newt. Fluid Mech.* 12:233–241.

46. Zhu, C., and R. Skalak. 1988. A continuum model of protrusion of pseudopod in leukocytes. *Biophys. J.* 54:1115–1137.

47. Galbraith, C. G., and M. P. Sheetz. 1999. Keratocytes pull with similar forces on their dorsal and ventral surfaces. *J. Cell Biol.* 147:1313–1324.

48. Charras, G. T., M. Coughlin, T. J. Mitchison, and L. Mahadevan. 2008. Life and times of a cellular bleb. *Biophys. J.* 94:1836–1853.

49. Lewis, A. K., and P. C. Bridgman. 1992. Nerve growth cone lamellipodia contain two populations of actin filaments that differ in organization and polarity. *J. Cell Biol.* 119:1219–1243.

50. Munro, E., J. Nance, and J. R. Priess. 2004. Cortical flows powered by asymmetrical contraction transport PAR proteins to establish and maintain anterior-posterior polarity in the early C. elegans embryo. *Dev. Cell.* 7:413–424.

51. Paluch, E., M. Piel, J. Prost, M. Bornens, and C. Sykes. 2005. Cortical actomyosin breakage triggers shape oscillations in cells and cell fragments. *Biophys. J.* 89:724–733.

52. Janson, L. W., J. Kolega, and D. L. Taylor. 1991. Modulation of contraction by gelation/solation in a reconstituted motile model. *J. Cell Biol.* 114:1005–1015.

53. DiMilla, P. A., K. Barbee, and D. A. Lauffenburger. 1991. Mathematical model for the effects of adhesion and mechanics on cell migration speed. *Biophys. J.* 60:15–37.

54. Anderson, K. I., and R. Cross. 2000. Contact dynamics during keratocyte motility. *Curr. Biol.* 10:253–260.

55. Kolega, J., M. S. Shure, W. T. Chen, and N. D. Young. 1982. Rapid cellular translocation is related to close contacts formed between various cultured cells and their substrata. *J. Cell Sci.* 54:23–34.

56. Choi, C. K., M. Vicente-Manzanares, J. Zareno, L. A. Whitmore, A. Mogilner, et al. 2008. Actin and α-actinin orchestrate the assembly and maturation of nascent adhesions in a myosin II motor-independent manner. *Nat. Cell Biol.* 10:1039–1050.

57. Bershadsky, A. D., C. Ballestrem, L. Carramusa, Y. Zilberman, B. Gilquin, et al. 2006. Assembly and mechanosensory function of focal adhesions: experiments and models. *Eur. J. Cell Biol.* 85:165–173.

58. Jurado, C., J. R. Haserick, and J. Lee. 2005. Slipping or gripping? Fluorescent speckle microscopy in fish keratocytes reveals two different mechanisms for generating a retrograde flow of actin. *Mol. Biol. Cell.* 16:507–518.